



## Oil detection in the coastal marshes of Louisiana using MESMA applied to band subsets of AVIRIS data



Seth H. Peterson<sup>a,\*</sup>, Dar A. Roberts<sup>a</sup>, Michael Beland<sup>a,b</sup>, Raymond F. Kokaly<sup>c</sup>, Susan L. Ustin<sup>d</sup>

<sup>a</sup> Department of Geography, UC Santa Barbara, CA 93106, USA

<sup>b</sup> Department of Geography, San Diego State University, CA 92182, USA

<sup>c</sup> U.S. Geological Survey, MS 973, Box 25046, Denver, CO 80225, USA

<sup>d</sup> Department of Land, Air, and Water Resources, University of California, Davis, Davis, CA 95616, USA

### ARTICLE INFO

#### Article history:

Received 30 July 2014

Received in revised form 16 December 2014

Accepted 18 December 2014

Available online 9 January 2015

#### Keywords:

Hyperspectral

Ecosystem disturbance and response

Oil spill

### ABSTRACT

We mapped oil presence in the marshes of Barataria Bay, Louisiana following the Deepwater Horizon oil spill using Airborne Visible InfraRed Imaging Spectrometer (AVIRIS) data. Oil and non-photosynthetic vegetation (NPV) have very similar spectra, differing only in two narrow hydrocarbon absorption regions around 1700 and 2300 nm. Confusion between NPV and oil is expressed as an increase in oil fraction error with increasing NPV, as shown by Multiple Endmember Spectral Mixture Analysis (MESMA) applied to synthetic spectra generated with known endmember fractions. Significantly, the magnitude of error varied depending upon the type of NPV in the mixture. To reduce error, we used stable zone unmixing to identify a nine band subset that emphasized the hydrocarbon absorption regions, allowing for more accurate detection of oil presence using MESMA. When this band subset was applied to post-spill AVIRIS data acquired over Barataria Bay on several dates following the 2010 oil spill, accuracies ranged from 87.5% to 93.3%. Oil presence extended 10.5 m into the marsh for oiled shorelines, showing a reduced oil fraction with increasing distance from the shoreline.

© 2014 Elsevier Inc. All rights reserved.

### 1. Introduction

The Mississippi River delta and associated marshes accumulated land area for 7000 years (~30,000 km<sup>2</sup>; Roberts, 1997), until about 1930. Since then, approximately 5000 km<sup>2</sup> of coastal wetlands have disappeared (Barras et al., 2003). Levees built throughout the 1900s have sharply reduced overbank flow into the delta, which stresses the vegetation because river water contributes sediment for marsh plants to grow on, nutrients to enhance productivity and health, and fresh water to reduce salinity stress from Gulf water (Day et al., 2000). Stressed vegetation that later dies leads to wetland loss, as the roots no longer have the ability to consolidate soil (Mendelssohn et al., 2012).

Periodic small-scale oil spills have been common in Louisiana salt marshes, and the effect of oil on them is well studied, though with differing conclusions, owing to different levels and timing of oiling, and even intraspecific variability in response to oil (Pezeshki, Hester, Lin, & Nyman, 2000; Webb, 1994). Oil affects salt marsh vegetation in a number of ways. When oil comes in direct contact with foliage it can block stomata, which 1) reduces transpiration and thus increases

temperature stress; 2) reduces photosynthesis by restricting CO<sub>2</sub>; and 3) reduces oxygen transport to the roots, which is critical for wetland plants (studies reviewed in Pezeshki et al., 2000). When unweathered oil is mixed with water and covers the soil it can reduce photosynthesis and plant stem density during the current growing season, and kill plants in the following growing season at fairly low concentrations (Lin & Mendelssohn, 1996). Preliminary results seven months after the Deepwater Horizon (DWH) oil spill demonstrate that aboveground live biomass was comparable for *Spartina alternifolia* (SPAL) in areas of moderate oiling, but sharply reduced for *Juncus roemerianus* (JURO), relative to control plots; in areas of heavy oiling there was minimal live biomass for either species (Lin & Mendelssohn, 2012). In addition, Lin and Mendelssohn (2012) performed a laboratory experiment using artificially weathered DWH oil, applying different levels of oil to foliage, and also oil to the soil. After 3 weeks the foliage showed less photosynthesis, proportional to the amount of oiling, while plants whose soil was oiled showed no decrease. After seven months, SPAL plants that had foliage (but not soil) oiled had largely recovered, whereas the plants that had their soil oiled showed 60% less photosynthesis than the control. In general, plants whose foliage is oiled often recover, but plants whose roots become exposed to oil often die (Mendelssohn et al., 2012). Ironically, post-spill cleanup can be as damaging to the marshes as the oil itself (Lin & Mendelssohn, 1998), thus 73% of the beaches that were oiled by the DWH oil spill

\* Corresponding author. Tel.: +1 805 893 4434.

E-mail address: [seth@geog.ucsb.edu](mailto:seth@geog.ucsb.edu) (S.H. Peterson).

were authorized to be cleaned but only 9% of the oiled marshes were so authorized (Michel et al., 2013).

The DWH oil rig began to leak on April 20, 2010, and was not closed until July 15. Over the course of the spill 4.4 million barrels of oil leaked into the Gulf of Mexico (Crone & Tolstoy, 2010). The northern Barataria Bay region experienced the majority of the oiling (Kokaly et al., 2013; Lin & Mendelssohn, 2012), with shoreline oiling occurring between May and September (Michel et al., 2013). Predicting the effect of the spill on the marshes of southern Louisiana begins with identifying the areas affected by oil. In this instance, oil was manually mapped using Shoreline Cleanup Assessment Technique (SCAT) protocols. Some 31,000 km of shoreline were surveyed (7058 unique km) by 18 teams over 7000 SCAT team-days in order to map oil presence/absence in Louisiana, Mississippi, Alabama, and northern Florida. A common argument for the use of remote sensing is that it is more efficient than field work when studying larger areas. If remote sensing can generate a map of oil approaching the accuracy of a SCAT map it would be an invaluable time saver. Additionally, SCAT teams only examined shorelines, remote sensing allows for the quantification of depth of oil penetration, laterally into the marsh from shore.

Hyperspectral remote sensing is an ideal tool to study oil spills because the spectral resolution allows for the detection of oil absorption features (Cloutis, 1989; Kokaly et al., 2013). Extensive Airborne Visible InfraRed Imaging Spectrometer (AVIRIS) flights occurred in the area following the oil spill, primarily from May to October 2010 and from May to October 2011 (data available at [http://aviris.jpl.nasa.gov/alt\\_locator/](http://aviris.jpl.nasa.gov/alt_locator/)). The many compounds in hydrocarbons result in 2 major absorption features: between 1650 and 1750 nm and between 2200 and 2600 nm, with the feature beginning at 2200 nm being particularly prominent (Cloutis, 1989). Thin oil films on water do not exhibit these features because of the low reflectance of water beyond 1100 nm (Clark et al., 2010; Wettle, Daniel, Logan, & Thankappan, 2009), however once an oil spill reaches land it becomes readily detectable (Kokaly et al., 2013). It should be noted that Horig, Kuhn, Oschutz, and Lehmann (2001) found the 1700 nm absorption feature to be stronger than the 2300 nm feature, and hence developed the Hydrocarbon Index solely using the 1700 nm feature (Kuhn, Oppermann, & Horig, 2004), however they used radiance data, not reflectance data, and reflected radiance is low at 2300 nm, reducing the prominence of that feature. Kokaly et al. (2013) used both features for oil detection, with the 2300 nm feature weighted 75% and the 1700 nm feature 25%.

Spectral Mixture Analysis (SMA) is a technique that transforms the digital number or reflectance values of a pixel into percentages of scene components, called endmembers (EMs). A typical vegetated area would be comprised of a mixture of three to four EMs: green vegetation (GV), non-photosynthetic vegetation (NPV), shadows/shade, and perhaps soil (Roberts, Smith, & Adams, 1993). The ability to discriminate different materials improves with greater spectral sampling, resulting in improvements in accuracy and the ability to discriminate materials using AVIRIS that cannot be readily discriminated by a broad band sensor, such as separating soils from NPV (Goetz & Boardman, 1989; Roberts et al., 1993). However, the high degree of similarity between oil and NPV spectra may confound SMA, prompting the following questions:

- 1) Is there a detection threshold for oil, or an amount of NPV presence where the level of certainty of oil fractions diminishes?
- 2) Is there a spectral band subset that can overcome the NPV/oil similarity issue?

The final goal of this research is to produce maps of oiled marsh having the highest possible accuracy.

## 2. Background

EM fractions are most accurate when the correct number and type of EMs are used to model each pixel (Sabot, Gillespie, Adams, Smith, & Tucker, 2002). For instance, the marshes of southern Louisiana include

woody areas that are a mix of mangrove GV, stem bark NPV, and shade; and salt marshes that are a mix of grass GV or grass NPV (depending on the season), and shade. Multiple EM SMA or MESMA allows both the number and type of EMs to vary on a per-pixel basis across the scene. MESMA can be performed on multispectral data (e.g. Peterson & Stow, 2003) but is most commonly performed on hyperspectral data (e.g. Roberts et al., 1998).

Recent research has focused on the use of band subsets when using SMA/MESMA with hyperspectral data (e.g. Asner & Lobell, 2000; Somers et al., 2010). Using a subset of hyperspectral bands was proposed by Sabot, Adams, and Smith (1992) and Roberts et al. (1993), and fully implemented by Asner and Lobell (2000). The objective is not to simply reduce the number of bands by convolving hyperspectral data to mimic Landsat bands, but rather, to choose specific wavelengths to target specific absorption features, and utilize those bands that maximize interclass separability and minimize intraclass variability. For instance, when looking at the Gulf oil spill, naturally senesced NPV and oil-coated vegetation have remarkably similar spectra, differing only in the oil absorption regions of 1700 and 2300 nm (Kokaly et al., 2013). AVIRIS data consist of 224 bands, of which we used 172 due to the removal of bands sensitive to water vapor absorption and bands with low signal-to-noise ratios. The two oil features are each on the order of 10 bands wide. Hence, when using 172 bands, only 10% of the bands are sensitive to oil. If the number of bands is reduced, particularly in wavelengths less than 1700 nm, the likelihood of identifying oil if it is present could be enhanced.

Asner and Lobell (2000) used the Short-wave-infrared (SWIR2: 2000–2500 nm) for unmixing as that spectral region maximized separability between NPV and soil for their semi-arid study area. They further reduced EM spectral variability through brightness normalizing the EMs by subtracting the reflectance at the first band in the SWIR2 from all other bands, for each spectrum. Hence, differences in spectral shape are emphasized over differences in average brightness. The technique was later updated, adding visible and NIR (near-infrared: 690–740 nm) regions so that it would work in more landscapes (Somers, Asner, Tits, & Coppin, 2011). A number of statistical band selection techniques have been proposed, reviewed in Somers et al. (2011), though none have achieved widespread usage to date. Stable zone unmixing (SZU; Somers et al., 2010) identifies which bands to use in SMA using an instability index (ISI), which is calculated as the ratio between within-class and between-class EM variability. For two EM mixing, ISI at wavelength  $i$  is calculated as:

$$ISI_i = 1.96 \left( \sigma_{1,i} + \sigma_{2,i} \right) / \left| \rho_{\text{mean},1,i} - \rho_{\text{mean},2,i} \right| \quad (1)$$

where  $\sigma_{1,i}$  and  $\sigma_{2,i}$  are the standard deviations at wavelength  $i$  for EM classes 1 (e.g. oil) and 2 (e.g. NPV), and  $\rho_{\text{mean},1,i}$  and  $\rho_{\text{mean},2,i}$  are mean reflectances for classes 1 and 2 at wavelength  $i$ . ISI is calculated for all of the bands, the values are sorted, and the difference between adjacent ISI values ( $d_{ISI,i}$ ) is calculated. Bands with the lowest  $ISI_i$  are removed first, and bands continue to be removed as long as accuracy increases. Somers et al. (2010) tested the ability of the SZU algorithm to unmix synthetic mixtures of EMs for six datasets. For three datasets,  $R^2$  was near 0.9 when all bands were used, and increased slightly when a subset was used; for the remaining datasets  $R^2$  increased from 0.41 to 0.68, 0.13 to 0.69, and 0.48 to 0.8, respectively. Testing an algorithm on synthetic mixtures is ideal because the exact fractions used to create the mixtures are known, and hence the ability to reproduce those fractions can be tested. Knowing exact EM percentages in real world imagery is uncommon.

The purpose of this research was to utilize the ISI statistic proposed by Somers et al. (2010) for band subset selection to identify and map oil, GV, and NPV using MESMA applied to AVIRIS data of the Barataria Bay region of Louisiana following the 2010 Gulf oil spill. One improvement to the Somers et al. (2010) method was brightness normalization of

EM spectra so that ISI was solely dependent on spectral shape. The equation for brightness normalizing is as follows:

$$\rho_{ni} = \rho_i / \text{average brightness} * \text{scale factor} \quad (2)$$

where

$$\text{average brightness} = \sqrt{\sum_{i=1}^N \rho_i^2}$$

where  $\rho_{ni}$  is the normalized reflectance,  $\rho_i$  is the original reflectance, and scale factor is 55% for GV, 80% for NPV, and 25% for oil; the values of the scale factors were chosen so as to re-scale the average brightness normalized spectra back to near their original reflectance values for each EM type (Fig. 1).

### 3. Material and methods

#### 3.1. Study area

The Barataria Bay region of southern Louisiana was the focus of this study because of the extent of Deepwater Horizon oil reaching the

shoreline (Kokaly et al., 2013; Lin & Mendelssohn, 2012). The region is comprised of approximately 5720 km<sup>2</sup> of open salt water with wetlands attached to the mainland and also occurring on islands in the bay. The wetland vegetation is dominated by SPAL, with JURO and *Distichlis spicata* (DISP) intermixed (Kokaly et al., 2013).

#### 3.2. AVIRIS data reflectance and geometric processing

AVIRIS data were collected for Barataria Bay on May 6, July 31, and August 24, 2010, and August 15, 2011 from the NASA ER-2 aircraft at altitudes of 19.7 (May) and 9.1 km (July and August), respectively. AVIRIS was also deployed on the Twin Otter on September 14, and October 4, 2010, and May 4 and October 15, 2011 at aircraft altitudes of 4.1, 4.1, 3.9, and 4.0 km, respectively. AVIRIS radiance data were atmospherically corrected and processed to apparent surface reflectance using mode 1.5 of the Atmospheric Correction Now (ACORN) radiative transfer program (ImSpec LLC, Palmdale, CA). Reflectance spectra of a calibration site, an airport tarmac, were acquired using an ASD Field Spec Pro (Analytical Spectral Devices, Boulder, CO) on June 27, 2010. These field-measured data were used to remove residual atmospheric features in the apparent surface reflectance data using ACORN mode 2 (Clark et al., 2002). Some bands remained unusable due to atmospheric

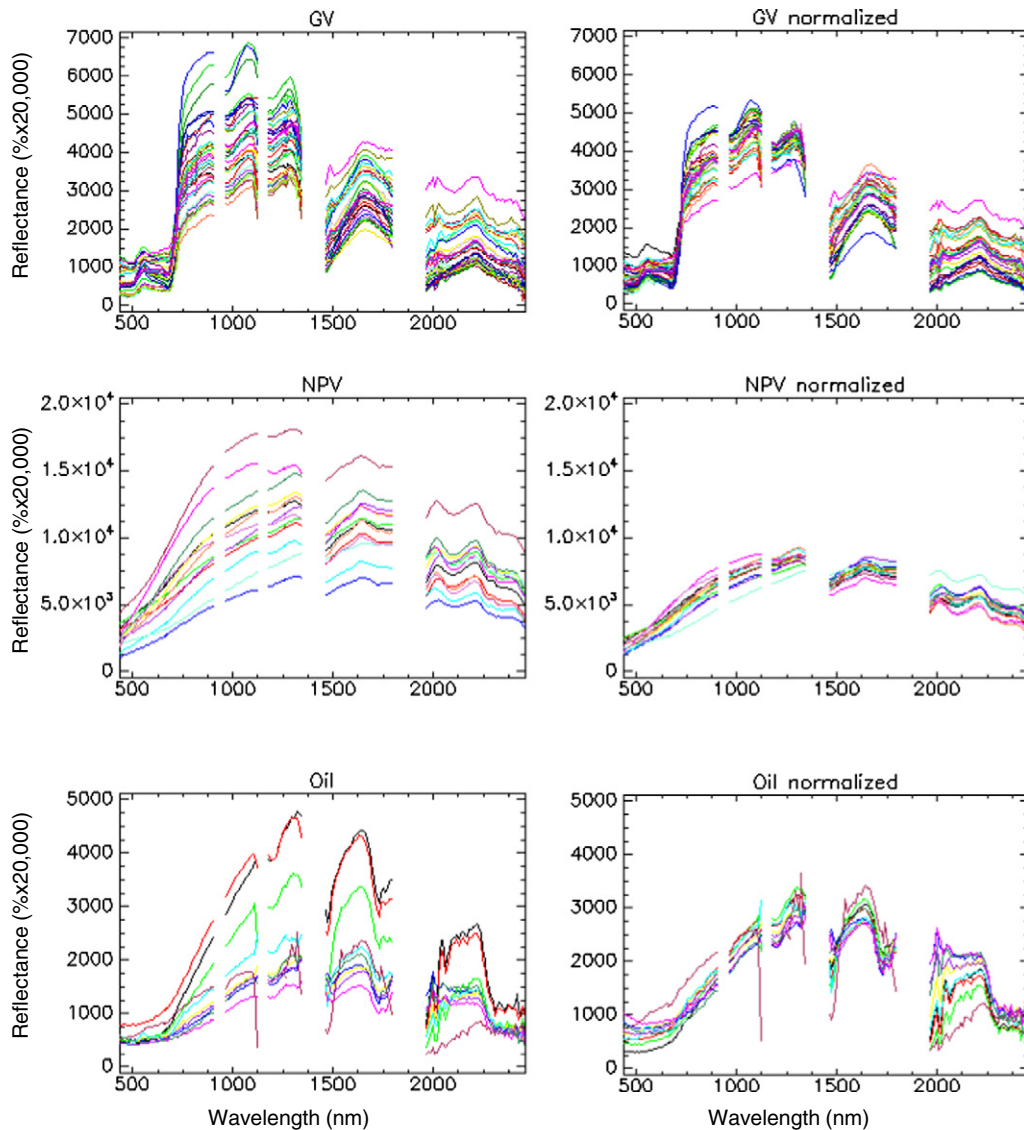


Fig. 1. Original (left) and brightness normalized (right) endmember (EM) spectra for green vegetation (GV), non-photosynthetic vegetation (NPV) and oil (top to bottom). Y-axes are not constant so that spectral features can be more easily discerned. Reflectance between 0 and 100% is scaled 0 to 20,000 on the y-axis.

water vapor or poor signal-to-noise ratio, the following bands were removed: 1–7, 59–64, 82–86, 107–117, 152–170, and 221–224.

Flight lines were delivered with a preliminary geometric correction (Boardman, 1999) and georeferenced to a mosaic of National Agriculture Imagery Program (NAIP) air photos from 2010 that were resampled to 6 m. Approximately 30 to 40 ground control points were generated between each flightline and the NAIP base map, and flightlines were warped with an average accuracy of 1–2 pixels. The September and October imagery were acquired such that there is a data gap between flight lines in the central-east portion of Barataria Bay (see Kokaly et al., 2013).

### 3.3. Synthetic mixture modeling

A spectral library containing GV, NPV, and oil EMs was generated in order to perform the synthetic mixture modeling. For GV, we used 23 SPAL image-derived EMs from both May 6 and September 14, 2010 AVIRIS imagery. Polygons of SPAL were identified by the Coastwide Reference Monitoring System (CRMS) program, all of the pixels were extracted from each polygon, and unique spectra were identified using iterative EM selection (IES: Roth, Dennison, & Roberts, 2012). Because oiling was limited to the immediate coastal regions, only SPAL spectra were used in this analysis. For NPV, we used 13 ASD reflectance spectra acquired on July 8 and August 13 and 14, 2010. For oil we used the Hydrocarbon Index (Kuhn et al., 2004) to identify candidate EMs in September 14, 2010 AVIRIS imagery, then selected eight image EMs that evidenced moderate to deep oil absorption features. Lastly, photometric shade of 0% reflectance was used. The EM spectra were brightness normalized to emphasize spectral shape and remove the importance of differences in average brightness (Fig. 1). For instance, if a non-normalized dark EM was best modeled by a non-normalized bright EM plus shade, the synthetic and modeled EM fractions would be different even though the root mean squared error (RMSE) was low, erroneously suggesting that the best set of modeled EM fractions was off of the 1:1 line.

Synthetic mixtures were generated using GV fractions of 50, 40, 30, 20 and 10% and NPV and oil fractions of 24, 18, 12, 6 and 0%. These values were empirically determined as they are roughly representative of actual EM fractions in the landscape. The number of levels was chosen to balance representativeness and computational efficiency. Gaussian noise (1%) was added to the mixtures so that variability was not entirely removed.

For each synthetic mixture all possible EMs (minus the actual EMs used to generate the mixed spectrum) were evaluated and the best model (based on RMSE) and its associated EM fractions was returned. We report the average modeled EM fractions from the 2392 (i.e.,  $23 \times 8 \times 13$ ) model runs with each fraction combination (e.g., 0.50 GV, 0.24 NPV, 0.24 oil).

### 3.4. Ideal band subset identification

Model selection in SMA/MESMA, which uses RMSE as a goodness-of-fit measure, may produce erroneous EM fractions when using the whole spectrum (172 bands) for materials that are spectrally similar because each band is equally weighted, diluting the enhanced separability that may be present only in narrow spectral regions (Sabol et al., 1992). To address this issue, we targeted spectral regions of interest for separating GV/NPV/oil. We calculated ISI values for NPV/oil, NPV/GV, and oil/GV for all 172 bands. We searched for local maxima in ISI values for NPV/oil and the sum of the three ISIs, seeking to maximize both NPV/oil and overall separability. This led to the identification of 17 bands that showed peaks in ISI values (Table 1). We performed a full synthetic mixture analysis using 17 bands, then iteratively removed one band at a time (backward stepwise analysis) until we identified a subset that maximized the  $R^2$  between synthetic and modeled oil EM spectra using the maximum NPV fraction (0.24) in order to maximize separability between oil and NPV.

**Table 1**

The 17 bands that were identified through ISI as being important for differentiating among GV, NPV, and oil. Using the nine bands in bold led to the highest accuracy in predicting oil amount.

Wavelength, nm	Spectral region
570	Visible – green
<b>685</b>	Visible – red
715	Near infrared
899	Near infrared
1111	Near infrared
<b>1263</b>	Near infrared
1512	Short wave infrared 1
<b>1622</b>	Short wave infrared 1
<b>1732</b>	Short wave infrared 1
<b>1772</b>	Short wave infrared 1
<b>2038</b>	Short wave infrared 2
2117	Short wave infrared 2
<b>2208</b>	Short wave infrared 2
<b>2238</b>	Short wave infrared 2
<b>2278</b>	Short wave infrared 2
2327	Short wave infrared 2
2377	Short wave infrared 2

### 3.5. Oil mapping

Following the identification of a good band subset through synthetic mixture modeling, MESMA was applied to all Barataria Bay flight lines in 2010 (7/31, 8/24, 9/14, 10/4) and 2011 (5/4, 8/15, 10/15). All two, three, and four EM models were run (GV/shade, NPV/shade, oil/shade; GV/NPV/shade, GV/oil/shade, NPV/oil/shade; GV/NPV/oil/shade). Then, on a pixel by pixel basis the best two and three EM model combinations were identified and the best two, three and four EM models were merged using an empirically derived threshold of 0.007 improvement in RMSE to choose a higher order model (i.e. more endmembers used to model a pixel; Roberts, Quattrochi, Hulley, Hook, & Green, 2012). The threshold is necessary because adding an additional variable (an EM in this case) will always improve model fit to some extent, regardless of whether the improvement is meaningful. The EM library that was used in the synthetic mixing experiment was modified slightly for the MESMA analysis. Additional GV EMs (four each from July 31 and August 24, and eight from October 4) were added so that there were SPAL spectra from each date to account for phenological variability (Dennison & Roberts, 2003). NPV and oil EMs remained the same for all images. The final EM fraction images for each date were resampled to a common pixel size of 3.5 m using nearest neighbor resampling, and resized to a common spatial extent for comparison purposes.

### 3.6. Map accuracy assessment

Shoreline surveys were conducted in July and August of 2010, identifying 32 oiled and 16 un-oiled shoreline sites (Kokaly et al., 2011). Field survey points where oil coated vegetation and oil-damaged vegetation canopies were present were considered oiled, while sites that either showed no oil or in which the oil was only present on stems but did not affect plant health were considered un-oiled (Kokaly et al., 2013; mapped in Fig. 7, therein). The presence of clouds and data gaps reduced the sample size slightly for the July, September, and October image dates for the reference data set; the number of validation points is 45, 48, 41, and 43, respectively for the four 2010 images. Identifying ground control points in the changing and relatively feature-less marsh was difficult, so geolocation errors exist in the AVIRIS data, and GPS readings for site location have ~5 m of uncertainty. Hence, we used a  $3 \times 3$  pixel window about each oiled shoreline site, if oil occurred anywhere with the window the site was considered to have oil. Additionally, where systematic errors were clear, i.e. if the GPS point for the site fell either in the marsh interior or offshore of the shoreline, the point was moved to

the shoreline. Additionally, of the 32 oiled sites, 25 also reported the depth of penetration of oil into the marsh.

### 3.7. Endmember trajectories for distance from shoreline

In order to summarize and interpret the EM fraction maps, EM fractions were averaged in terms of distance from the shoreline for oiled/oil-free shoreline (as per Khanna et al., 2013). The September 2010 image was used as it had the highest native pixel resolution and amount of oil detected. Land pixels were empirically identified as having a GV or oil EM fraction above 0.05 or NPV above 0.2. A 5% error threshold is common when performing MESMA (Roberts et al., 1998); a higher threshold was needed for NPV owing to the presence of small amounts of NPV where sun glint on water was present. The land raster was converted to a polygon coverage, and Euclidean distance and direction from the boundary between land and water were calculated for each pixel using ArcMap 10.2. Twelve 3.5 m zones from the shoreline are reported as values converged at that point. Oiled shoreline pixels were identified by having an oil EM fraction greater than 0.05 and being within zone 1. Oil-free shoreline pixels were identified as having an oil EM fraction less than 0.05, being within zone 1, within 100 m of an oiled pixel, and also being on a generally southerly facing shoreline (between 70 and 290°). The 100 m and southerly constraints assure that environmental conditions are similar between oiled and oil-free pixels. Euclidean distances were calculated for the oiled/oil-free shoreline pixels to all other pixels and land pixels in zones 2–12 were assigned to the oiled or oil-free class based on minimum distance.

## 4. Results

### 4.1. Brightness normalized spectra

The spectra in the rightmost column of Fig. 1 have much less variability in brightness than the original spectra. This reduces EM variability due

solely to brightness and not spectral shape. It also reveals interesting patterns in the oil spectra. The original spectra show a range in values in NIR from ~1500 to ~5000 (reflectance scaled 1–10,000 for 1–100%). The normalized spectra show that the slopes from 600 nm to 1200 nm are actually quite similar, and that the primary difference in the spectra lies in SWIR 2 (2000–2400 nm). The different depths in the oil absorption feature around 2300 nm are due to different degrees of oiling.

### 4.2. Synthetic mixture modeling

Plots from the model runs show oil fractions used to generate the mixture (x axis) plotted against modeled oil fractions (y axis) (Figs. 2 and 3). In almost all cases, an increase in NPV fraction led to an increase in error in modeled oil, either leading to a greater over estimate (Fig. 2b, c, e) or greater underestimate (Fig. 2a, d, f), i.e. there is a clear progression of estimated oil fractions away from the 1:1 line as NPV fraction increases in Fig. 2. The error varied depending upon both the NPV spectrum used in the synthetic mixture and the amount of NPV used. For instance, model results plotted in Fig. 2a and c, showed errors of less than 4% when comparing the 0% and 24% NPV cases. By contrast, the NPV spectrum used in model e generated an overestimate as large as 16%, and in model f an underestimate of similar magnitude. These results suggest that detection limits will depend on the type of NPV present in the mixture. For example, given a 4% over estimate, an oil fraction of 4% or more would be detectable. Given an overestimate of 16% (as shown in Fig. 2e), close to 20% oil would need to be present to detect it with confidence.

The averaged regression results for predicting oil fractions with a 0.24 fixed NPV fraction and different band subsets are presented in Table 2. Intercepts are all positive and close to 0, indicating a small over prediction of oil when the true oil fraction was 0%. The slopes deviate from a 1:1 line, being shallower, meaning that estimated oil fractions are lower than actual oil fractions for high values and/or higher than actual values at low oil values (see also Fig. 3). The slope and  $R^2$  when

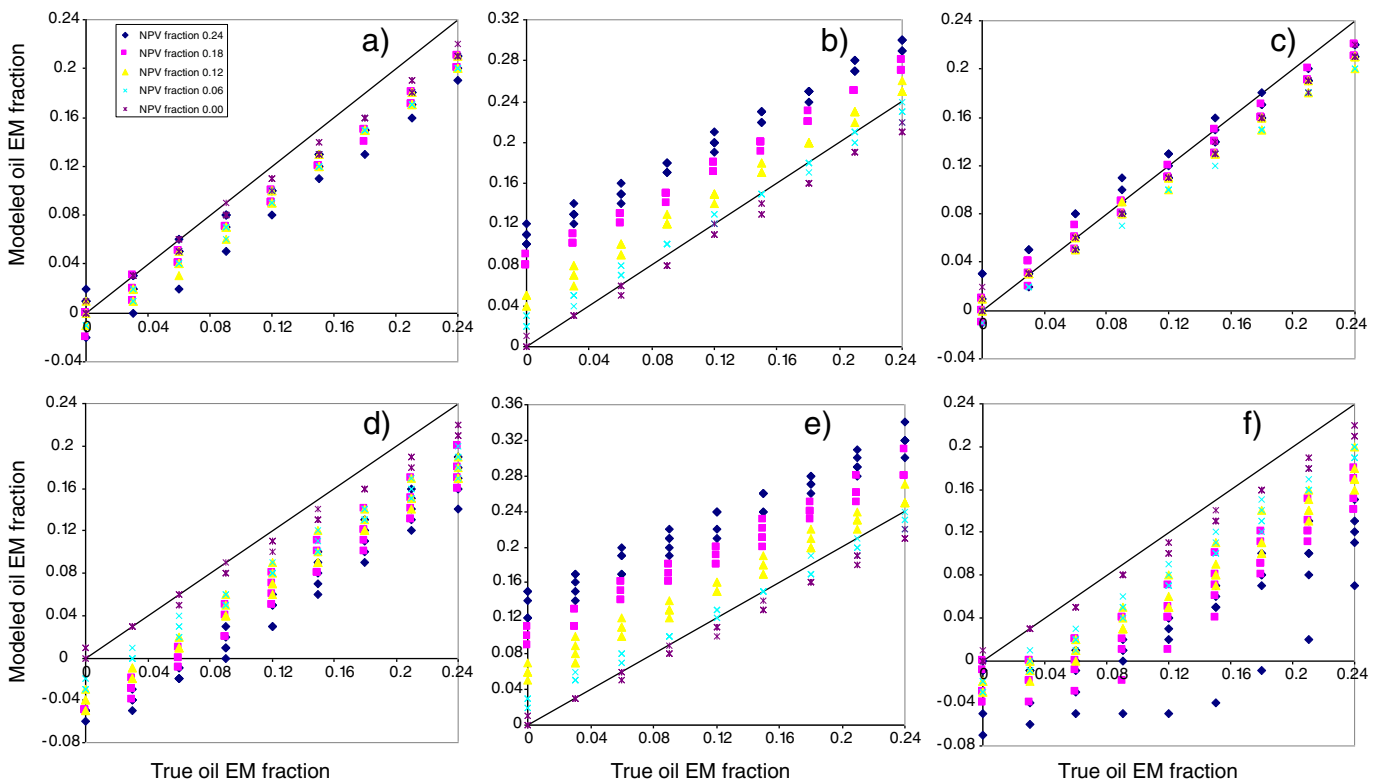
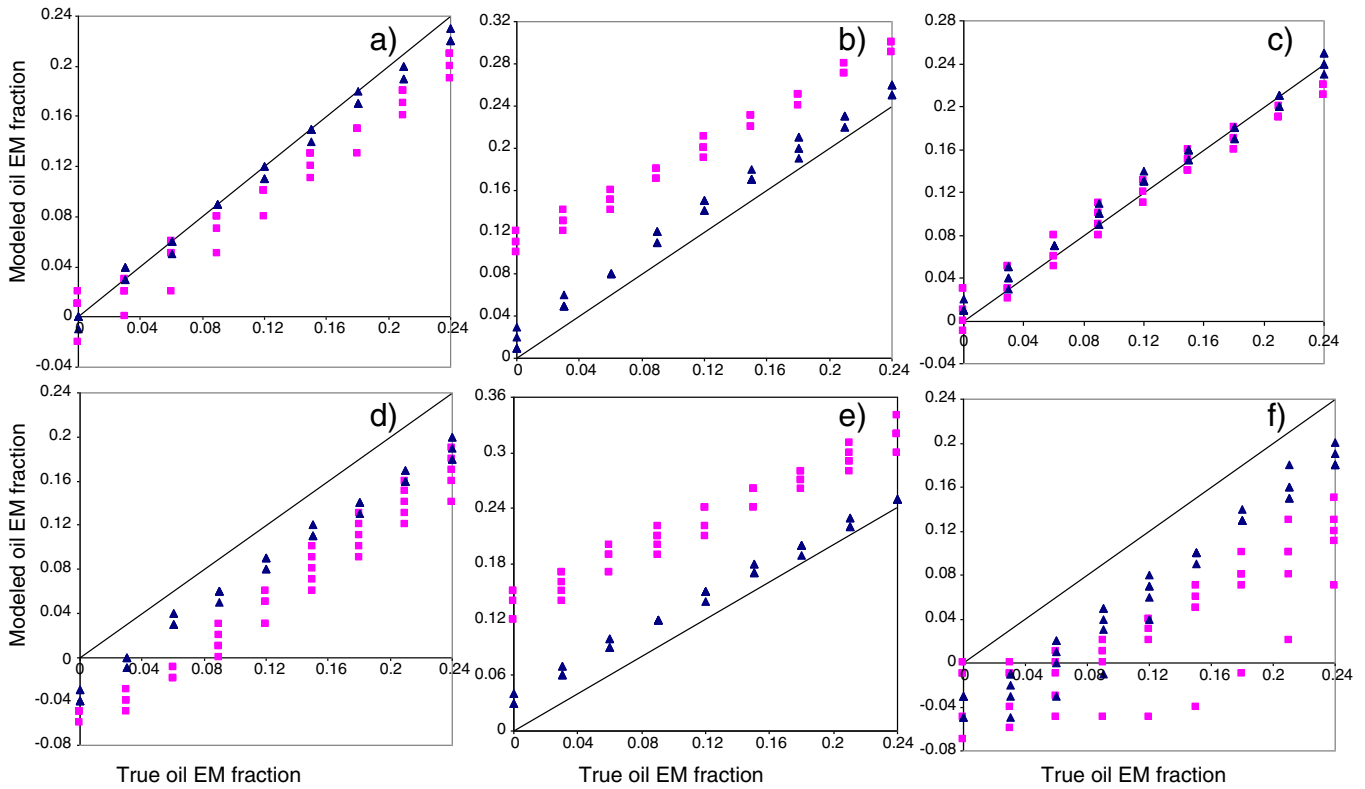


Fig. 2. Modeled (y axis) vs. true (x axis) oil EM fractions when NPV fraction was set to 0.24, 0.18, 0.12, 0.06, and 0. Variability and false positives/negatives in oil fraction increase as NPV fraction increases. Results for six of the eleven NPV EMs used in this study, numbered 0, 1, 4, 6, 10, and 11, are displayed in panels a–f.



**Fig. 3.** Modeled (y axis) vs. true (x axis) oil EM fractions when NPV fraction was set to 0.24, which had the greatest effect on oil fraction accuracy. The magenta data series are oil fractions generated by MESMA operating on the 172 good bands, the navy blue data series are oil fractions generated by MESMA operating on 9 bands targeted towards specific reflectance features of GV, NPV, and oil. Variability and false positives/negatives in oil fraction decrease notably under the reduced bands scenario. Plots are for NPV EMs numbered 0, 1, 4, 6, 10, and 11.

using all bands to estimate oil fraction were 0.817 and 0.953, respectively. When systematically reducing bands by choosing every nth band, slopes became steeper, but still did not approach 1:1. The slope and  $R^2$  values when using the 17 ISI identified bands were 0.859 and 0.956; the slope was improved over the full 172 band MESMA fractions, but  $R^2$  showed little change. The final nine band subset (Table 1) showed marked improvement; the intercept dropped from 0.023 to 0.011, the slope increased to 0.972, markedly closer to the 1:1 line than for any of the other scenarios, and scatter was reduced with an  $R^2$  of 0.979. Fig. 3 presents synthetic vs. modeled oil fractions for six of the eleven NPV EMs that were used to generate the synthetic mixtures. In this figure, magenta points show results using all 172 wavelengths, and blue

points those using the subset. In all cases the distance to the 1:1 line is smaller, and for most cases modeled oil fraction variability is reduced. This serves to reduce the impact of variability in the NPV EM used. It should be noted that the backward stepwise elimination did not locate a clear winner; a number of nine and ten band subsets had similar intercepts, slopes, and  $R^2$  values. We chose the band combination that also produced the best maps.

4.3. Oil mapping

To evaluate oil detection over time, the best wavelength subset was applied using MESMA to map oil for four dates in 2010 and three dates in 2011 for three areas in Barataria Bay (Figs. 4, 5, 6). Only the first 2011 date is shown in the figures due to lack of oil. Oiled shoreline was identified as areas having an estimated oil fraction greater than 5%. For the most part, where oil is present in 2010 it is present in all four image-dates of 2010, and there is much less oil in 2011 (e.g., Fig. 4). Accuracies for the four 2010 image dates ranged from 87.5% to 93.3%, with no false positives for oil detection (Table 3).

We illustrate three areas that show dynamic oil presence (Figs. 4, 5, 6). In the Bay Jimmy island area, there is a notable progression of oil moving down the northwest coast of the island and filling in the west coast through 2010; oil is much reduced by 2011, with only a slight amount of oil remaining on the northwest coast, where it had been widest in 2010 (Fig. 4). In contrast, on the west side of Barataria Bay, the maximum amount of oil was found in the July 31, 2010 image, with a steady reduction thereafter (Fig. 5). The subset from the central part of Barataria Bay shows approximately equal oiling throughout 2010 and minimal oil in May 2011, again in areas where it had been most common in 2010 (Fig. 6).

**Table 2**

Averaged regression results for oil endmember fraction from unmixing synthetic endmember spectra for a number of different combinations of AVIRIS bands. Using the nine band subset led to predicted oil fractions being closest to the oil fraction values used to generate the synthetic spectra.

Intercept	Slope	RSQ	Band combination
0.023	0.817	0.953	All 172
0.022	0.834	0.957	172/2
0.022	0.809	0.953	172/3
0.022	0.857	0.95	172/4
0.027	0.849	0.965	172/5
0.019	0.862	0.97	172/6
0.02	0.845	0.97	172/7
0.026	0.871	0.952	172/8
0.017	0.827	0.954	172/9
0.042	0.819	0.963	172/10
0.022	0.859	0.956	Best 17
0.011	0.972	0.979	Best 9

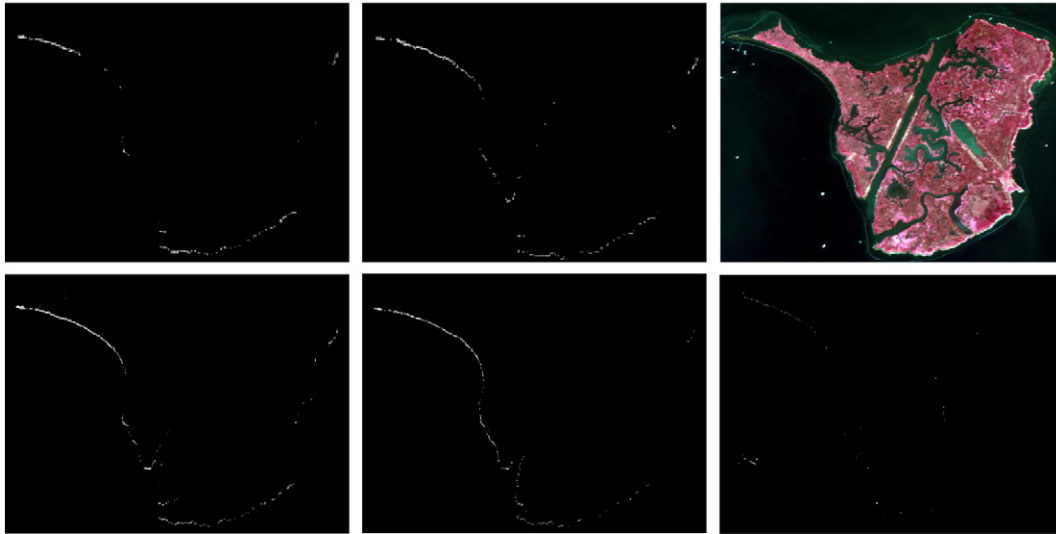


**Fig. 4.** Oil EM fraction Bay Jimmy area: a) 7/31, b) 8/24, c) NIR color composite 9/14 2010, d) 9/14, e) 10/4 2010, and f) 5/4 2011. You can see the progression of oil presence down the NW shore of the island thru 2010. Oil is less present in May 2011, and is largely gone in August and October 2011 (not shown).

Distance of oil penetration into the marsh is a more robust check on accuracy as it goes beyond presence/absence to a quantitative measure. Binary classification accuracy for the September 14 data was very good (92.7%); predictions of oil penetration distance into the marsh for the September 14 data are still quite good (Fig. 7). The  $R^2$  between actual and estimated penetration depth was 0.49,  $p$ -value 0.00039.

#### 4.4. Endmember trajectories

Endmember trajectories from the September 14th data show that oil effects were largely limited to zones 1–4, or within 14 m from the shoreline (Fig. 8). Oil-free pixels were largely comprised of GV and shade, with lower GV fractions in zone 1 nearest to the shore, indicating a mixture of vegetation and water there; NPV fractions were low, indicating that the marsh vegetation had not started senescing yet in September. Oiled pixels consisted of a mix of GV, oil, NPV, and shade. The higher values for NPV in zones 1–4 were likely due to oil stressing and killing the vegetation; the oil came ashore approximately three months prior

to the September image acquisition. Oil fraction decreases linearly with distance from shoreline; however, pixel counts of oiled pixels within each zone (998, 968, 879, 270, 36, 1, 1 respectively for zones 1 through 7) show a different pattern. This suggests that where shorelines were oiled, the oil extends 3 pixels into the marsh in most cases, though by zone 3 there begins to be less oil and more remaining living vegetation. Only 27% of oiled shoreline pixels had an oil zone extending 4 pixels into the marsh. There were minor amounts of oil in zones five to seven.

## 5. Discussion

The use of a subset of hyperspectral bands to better discriminate among and between EM types is a developing field of research and has been used in landscapes as diverse as semi arid rangelands, fruit orchards, and tropical rainforests (Asner & Lobell, 2000; Somers & Asner, 2013; Somers et al., 2010). Somers et al. (2010) found that  $R^2$  was near 0.9 for half of their data sets when all bands were used to evaluate canopy cover in fruit orchards, increasingly slightly for a subset

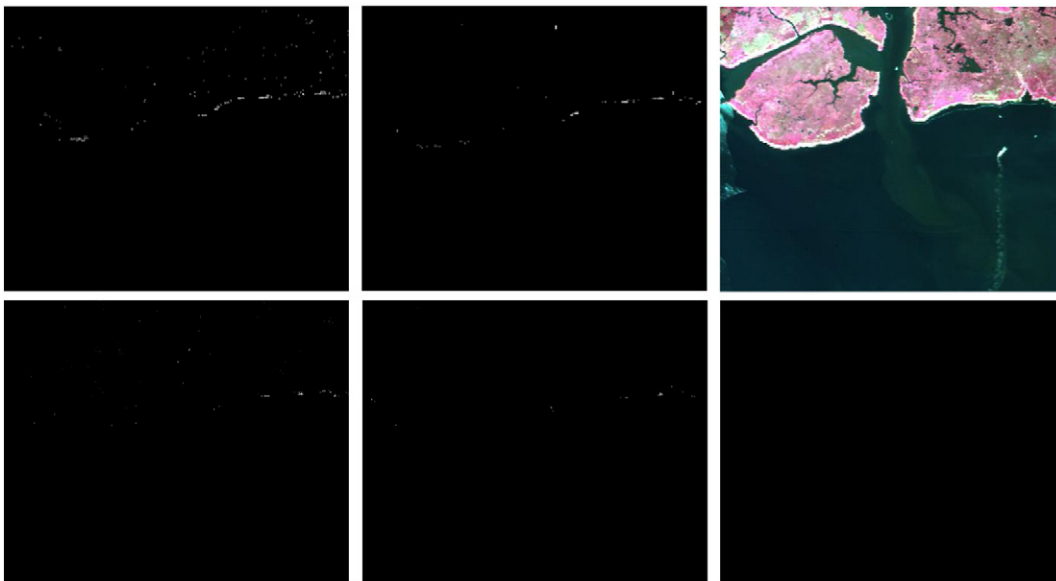


**Fig. 5.** Oil EM fraction in the far western Barataria Bay area: a) 7/31, b) 8/24, c) NIR color composite 9/14 2010, d) 9/14, e) 10/4 2010, and f) 5/4 2011. Oil is most present in July 2010, steadily decreasing the remaining 3 dates in 2010, and has largely disappeared in May 2011.

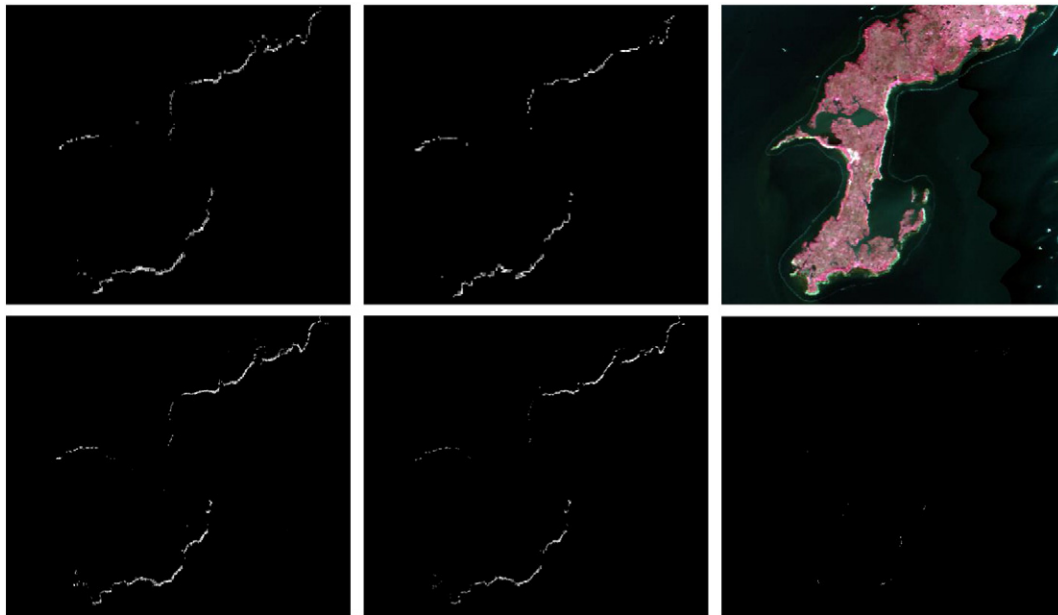


**Fig. 6.** Oil EM fraction in the central Barataria Bay area: a) 7/31, b) 8/24, c) NIR color composite 9/14 2010, d) 9/14, e) 10/4 2010, and f) 5/4 2011. Oiling is approximately equal throughout 2010, and has a much reduced extent in May 2011.

of bands selected by SZU. In the other half of their data, the R2 showed a much more substantial increase, equal to 0.38 on average. In our study, we also observed only modest increases in  $R^2$ , from 0.953 to 0.979, when the targeted bands were used as opposed to all 172. However, more importantly we also evaluated the effect of using a reduced number of bands on the slope and intercept of the regression for predicting oil fraction. Slope and intercept became much closer to the 1:1 line when fewer, targeted bands were used; 0.972 and 0.011 versus 0.817 and 0.023 for all bands, indicating a sharp reduction in systematic prediction errors. This is likely because in the full 172 band image, 20 bands were sensitive to oil absorption features, whereas in our final nine band image, six of the nine were sensitive to the oil absorption features.

We used the bands identified in the synthetic mixing step to map oil using MESMA in Barataria Bay, Louisiana. Oil map accuracy was slightly better than that found in Kokaly et al. (2013), with one to three additional sites being correctly classified on each image date. Examining the causes of misclassification is interesting. For the September 14th data, two of the three misclassified oiled sites showed oil two to three pixels from the survey point, which is beyond the  $3 \times 3$  pixel window threshold we used but within range of the residual georeferencing errors in the AVIRIS imagery and GPS. For the July 31 and October 4th data, georeferencing errors may explain one of the incorrectly classified sites. The remaining undetected oiled sites for July 31, September 14, and October 4 were described as having a small ( $1 \text{ m}^2$ ) oil patch or a narrow (1–3 m) fringe of shoreline oiling (Kokaly et al., 2011). This narrow oiling may have broken down in the 40 days between field sampling and image acquisition, or could have been undetected. Accuracy was lowest for the 24 August AVIRIS data, the date which had the largest native pixel resolution (7.7 m). Additional incorrectly identified oiled sites in the August data with respect to the other dates were described as having narrow (less than a 7.7 m pixel) fringes of oil (Kokaly et al., 2011), so MESMA for oil detection can break down when pixel size becomes much larger than patch size.

We had four dates of AVIRIS imagery in 2010, so we were able to identify temporal patterns in oiling (Figs. 4, 5, and 6). The field survey teams that led to the SCAT map visited shorelines in Barataria Bay two to five times in 2010. However, the vectors in their map are quite large, so it is difficult to identify temporal changes in oiling. For instance, the SCAT map showed uniform oiling on the northwest and west coast

of the island in Fig. 4 in 2010 while the AVIRIS-based maps showed a definite progression in oiling. Another benefit of having multiple image dates is it can be seen that only those areas that were oiled in all four dates retained some oil in 2011. This information is important because persistent oiling is more toxic, affecting the long-term recovery of the marsh (Lin & Mendelsohn, 2012).

The tidal range in Barataria Bay is minimal (30–40 cm), which led to shallow penetration of oil into the marsh vegetation (in the absence of storm events), given the nature of the oil spill. In the September 14th imagery, where oil occurred it tended to penetrate three zones (10.5 m) into the marsh (998 pixels in zone 1, 968 in zone 2, 879 in zone 3). Penetration into zone 4 was sharply reduced, only 27% of oiled shoreline pixels extended to zone 4 (14 m), and less than 1% extended farther. These values correspond well with values from a field survey of 34 oiled points: mean oil penetration was 6.7 m with a standard deviation of 4.5 m, and a maximum of 19 m (Kokaly et al., 2011). Similarly, the regression of measured and modeled oil penetration showed good agreement (Fig. 7,  $R^2$  of 0.49), especially given that some scatter is expected given the temporal disconnect between field sampling (July, August) and image acquisition (September), georeferencing errors in the AVIRIS imagery and GPS, and the fact that EM fractions reveal the percent of a pixel covered by the EM but not the spatial arrangement of the EM in the pixel.

**Table 3**

Oil detection accuracy when MESMA was applied to four dates of AVIRIS data in 2010, using the nine band subset.

AVIRIS image date	Remote sensing class	Reference class		User's accuracy	Overall accuracy
		Oil	Non-oil		
July 31, 2010	Oil	26	0	100.0%	93.3%
	Non-oil	3	16	84.2%	
	Producer's accuracy	89.7%	100.0%		
August 24, 2010	Oil	26	0	100.0%	87.5%
	Non-oil	6	16	72.7%	
	Producer's accuracy	81.3%	100.0%		
September 14, 2010	Oil	24	0	100.0%	92.7%
	Non-oil	3	14	82.4%	
	Producer's accuracy	88.9%	100.0%		
October 4, 2010	Oil	26	0	100.0%	93.0%
	Non-oil	3	14	82.4%	
	Producer's accuracy	89.7%	100.0%		

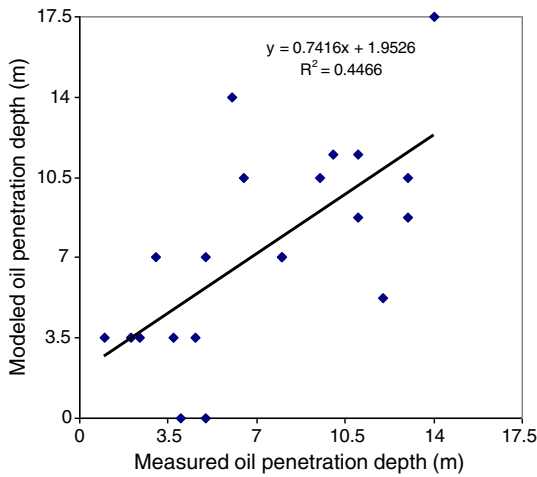


**Fig. 7.** Field measured oil penetration depth versus oil penetration depth in the 14 September AVIRIS imagery in pixels perpendicular to the shoreline, converted to meters. Oil penetration was measured for 20 of the 27 sites that appear in Table 3 for September 14 data, including two of the sites where oil was incorrectly not found in the imagery.

**6. Conclusion**

We demonstrated that there is an improvement in endmember fraction accuracy when using fewer bands to perform MESMA. We utilized the ISI statistic from Somers et al. (2010), replacing some of the automation in their SZU method with expert knowledge to target AVIRIS bands that have known absorption and transmission features for the endmembers of interest.

We mapped oil in coastal Louisiana following the DWH oil spill using AVIRIS imagery acquired in four dates in 2010 and one date in 2011. Many areas were heavily oiled in all four dates in 2010 as there was adequate time between the beginning of the spill (April 20) and the first image date (July 31) for oil to spread. Based on the time series, oil appeared to first come ashore in the western portion of Barataria Bay and then spread to the east. There was a sharp reduction in oil in the 2011 imagery.

Oiled shorelines in September 2010 were comprised of relatively equal proportions of living and senesced vegetation and oil. Oil fraction decreased linearly with distance from shoreline. GV fraction increased with distance from shoreline due both to the reduction of salt water and reduction in oil and NPV. Oil-killed vegetation was found in the same zones as oil, though the range in values was reduced with respect to oil. EM fractions showed minimal oiling effects at distances greater than 14 m from the shoreline.

Future research will determine how vegetation recovery and/or vegetation loss and shoreline retreat relate to three axes of oiling: oil EM fraction, depth of penetration into the marsh, and persistence in oiling through time.

**Acknowledgments**

The NASA AVIRIS team collected a very large amount of data in areas affected by the Gulf oil spill, which has been critical to this research and will be useful for many more research projects. This work was funded in part by grant NNX12AK58K from the NASA Terrestrial Ecology program entitled “Coastal Wetland and Near Shore Ecosystem Impacts from the Gulf of Mexico BP Horizon Oil Spill Monitored by NASA’s AVIRIS and MASTER Imagers” (Principal Investigator S. Ustin) and in part by a proposal to the NSF Rapid Grant Program entitled “Analysis of NASA’s Advanced Visible Infrared Imaging Spectrometer Data Acquired

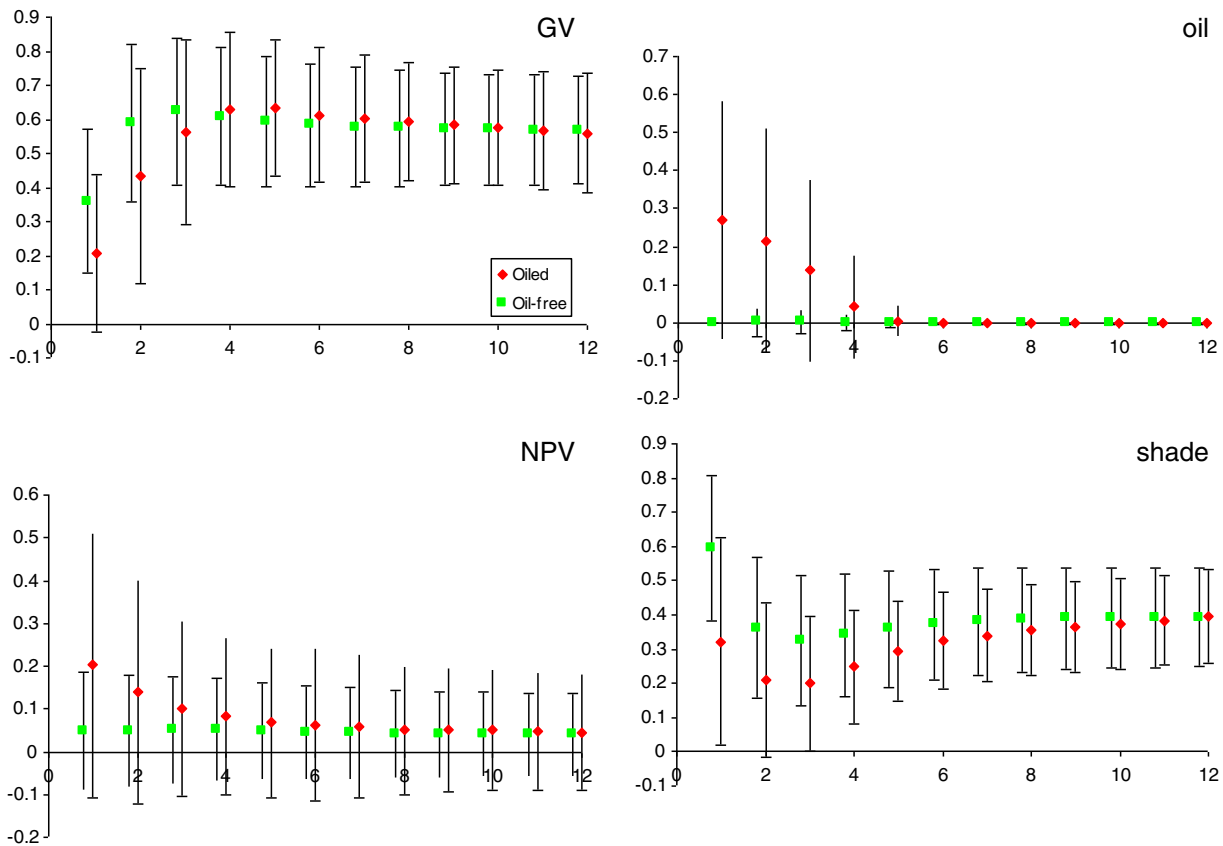


**Fig. 8.** Average endmember fraction values from the September 2010 imagery within twelve 3.5 m zones from the shore for oiled and oil-free shorelines. Oil fraction decreases linearly in the 17.5 m from the shore. NPV fractions in the first 14 m were higher than the ambient NPV fraction, indicating some vegetation senescence and mortality had occurred in the 4 months since oil began impacting Barataria Bay.

Over Multiple Dates and Flight lines along the Northern Gulf Coastline, including Barrier Islands,” (Principal Investigator S. Ustin). Any use of trade, product, or firm names is for descriptive purposes only and does not imply endorsement by the U.S. Government.

## References

- Asner, G.P., & Lobell, D.B. (2000). A biogeophysical approach for automated SWIR unmixing of soils and vegetation. *Remote Sensing of Environment*, 74, 99–112.
- Barras, J., Beville, S., Britsch, D., Hartley, S., Hawes, S., Johnston, J., et al. (2003). Historical and projected coastal Louisiana land changes: 1978–2050. *USGS Open File Report: OFR 03-334* (39 pp.).
- Boardman, J.W. (1999). Precision geocoding of low altitude AVIRIS data: Lessons learned in 1998. In R.O. Green (Ed.), *Summaries of the 8th JPL Airborne Earth Science Workshop. JPL publication 99-17*. (pp. 63–68). Pasadena, CA: Jet Propulsion Lab.
- Clark, R.N., Swayze, G.A., Leifer, I., Livo, K.E., Kokaly, R., Hoefen, T., et al. (2010). A method for quantitative mapping of thick oil spills using imaging spectroscopy. *U.S. Geological Survey Open-File Report 2010-1167* (51 pp.).
- Clark, R.N., Swayze, G.A., Livo, K.E., Kokaly, R.F., King, T.V.V., Dalton, J.B., et al. (2002). Surface reflectance calibration of terrestrial imaging spectroscopy data. In R.O. Green (Ed.), *Proceedings of the Eleventh JPL Airborne Earth Science Workshop. JPL Publication 03-04*. (pp. 43–64) (<http://speclab.cr.usgs.gov/PAPERS/calibration/tutorial/>).
- Cloutis, E.A. (1989). Spectral reflectance properties of hydrocarbons: Remote sensing implications. *Science*, 245(4914), 165–168.
- Crone, T.J., & Tolstoy, M. (2010). Magnitude of the 2010 Gulf of Mexico leak. *Science*, 330(6004), 634.
- Day, J.W., Britsch, L.D., Hawes, S.R., Shaffer, G.P., Reed, D.J., & Cahoon, D. (2000). Pattern and process of land loss in the Mississippi Delta: A spatial and temporal analysis of wetland habitat change. *Estuaries*, 23(4), 425–438.
- Dennison, P.E., & Roberts, D.A. (2003). The effects of vegetation phenology on endmember selection and species mapping in Southern California chaparral. *Remote Sensing of Environment*, 87, 295–309.
- Goetz, A.F.H., & Boardman, J.W. (1989). Quantitative determination of imaging spectrometer specifications based on spectral mixing models. *Proceedings of IGARSS 1989, Vancouver, British Columbia* (pp. 1036–1039).
- Horig, B., Kuhn, F., Oschutz, F., & Lehmann, F. (2001). HyMap hyperspectral remote sensing to detect hydrocarbons. *International Journal of Remote Sensing*, 22(8), 1413–1422.
- Khanna, S., Santos, M.J., Ustin, S.L., Koltunov, A., Kokaly, R.F., & Roberts, D.A. (2013). Detection of salt marsh vegetation stress and recovery after the Deepwater Horizon oil spill in Barataria Bay, Gulf of Mexico, using AVIRIS data. *PLoS ONE*, 8(11), e78989.
- Kokaly, R.F., Couvillion, B.R., Holloway, J.M., Roberts, D.A., Ustin, S.L., Peterson, S.H., et al. (2013). Spectroscopic remote sensing of the distribution and persistence of oil from the Deepwater Horizon spill in Barataria Bay marshes. *Remote Sensing of Environment*, 129, 210–230.
- Kokaly, R. F., Heckman, D., Holloway, J., Piazza, S., Couvillion, B., Steyer, G. D., et al. (2011). Shoreline surveys of oil-impacted marsh in southern Louisiana, July to August 2010. *U.S. Geological Survey Open-File Report 2011-1022* (124 pp., available at <http://pubs.usgs.gov/of/2011/1022/>).
- Kuhn, F., Oppermann, K., & Horig, B. (2004). Hydrocarbon index – an algorithm for hyperspectral detection of hydrocarbons. *International Journal of Remote Sensing*, 25(12), 2467–2473.
- Lin, Q., & Mendelsohn, I.A. (1996). A comparative investigation of the effects of south Louisiana crude oil on the vegetation of fresh, brackish, and salt marshes. *Marine Pollution Bulletin*, 32(2), 202–209.
- Lin, Q., & Mendelsohn, I.A. (1998). The combined effects of phytoremediation and biostimulation in enhancing habitat restoration and oil degradation of petroleum contaminated wetlands. *Ecological Engineering*, 10, 263–274.
- Lin, Q., & Mendelsohn, I.A. (2012). Impacts and recovery of the Deepwater Horizon oil spill on vegetation structure and function of coastal salt marshes in the northern Gulf of Mexico. *Environmental Science & Technology*, 46, 3737–3743.
- Mendelsohn, I.A., Andersen, G.L., Baltz, D.M., Caffey, R.H., Carman, K.R., Fleeger, J.W., et al. (2012). Oil impacts on coastal wetlands: Implications for the Mississippi River Delta ecosystem after the Deepwater Horizon oil spill. *Bioscience*, 62(6), 562–574.
- Michel, J., Owens, E.H., Zengel, S., Graham, A., Nixon, Z., Allard, T., et al. (2013). Extent and degree of shoreline oiling: Deepwater Horizon oil spill, Gulf of Mexico, USA. *PLoS ONE*, 8(6), e65087.
- Peterson, S.H., & Stow, D.A. (2003). Using multiple endmember spectral mixture analysis to study chaparral regrowth in southern California. *International Journal of Remote Sensing*, 24(22), 4481–4504.
- Pezeshki, S.R., Hester, M.W., Lin, Q., & Nyman, J.A. (2000). The effects of oil spill and clean-up on dominant US Gulf coast marsh macrophytes: A review. *Environmental Pollution*, 108, 129–139.
- Roberts, H.H. (1997). Dynamic changes of the Holocene Mississippi River delta plain: The delta cycle. *Journal of Coastal Research*, 13(3), 605–627.
- Roberts, D.A., Gardener, M., Church, R., Ustin, S., Scheer, G., & Green, R.O. (1998). Mapping chaparral in the Santa Monica Mountains using multiple endmember spectral mixture models. *Remote Sensing of Environment*, 65, 267–279.
- Roberts, D.A., Quattrochi, D.A., Hulley, G.C., Hook, S.J., & Green, R.O. (2012). Synergies between VSWIR and TIR data for the urban environment: An evaluation of the potential for the Hyperspectral Infrared Imager (HyspIRI) Decadal Survey mission. *Remote Sensing of Environment*, 117, 83–101.
- Roberts, D.A., Smith, M.O., & Adams, J.B. (1993). Green vegetation, nonphotosynthetic vegetation, and soils in AVIRIS data. *Remote Sensing of Environment*, 44(2–3), 255–269.
- Roth, K.L., Dennison, P.E., & Roberts, D.A. (2012). Comparing endmember selection techniques for accurate mapping of plant species and land cover using imaging spectrometer data. *Remote Sensing of Environment*, 127, 139–152.
- Sabol, D.E., Adams, J.B., & Smith, M.O. (1992). Quantitative subpixel detection of targets in multispectral images. *Journal of Geophysical Research*, 97, 2659–2672.
- Sabol, D.E., Gillespie, A.R., Adams, J.B., Smith, M.O., & Tucker, C.J. (2002). Structural stage in Pacific Northwest forests estimated using simple mixing models of multispectral images. *Remote Sensing of Environment*, 80, 1–16.
- Somers, B., & Asner, G.P. (2013). Multi-temporal hyperspectral mixture analysis and feature selection for invasive species mapping in rainforests. *Remote Sensing of Environment*, 136, 14–27.
- Somers, B., Asner, G.P., Tits, L., & Coppin, P. (2011). Endmember variability in spectral mixture analysis: A review. *Remote Sensing of Environment*, 115, 1603–1616.
- Somers, B., Delalieux, S., Verstraeten, W.W., van Aardt, J.A.N., Albrigo, G.L., & Coppin, P. (2010). An automated waveband selection technique for optimized hyperspectral mixture analysis. *International Journal of Remote Sensing*, 20(20), 5549–5568.
- Webb, J.W. (1994). Effects of oil on saltmarshes. *Symp. Proc. Gulf of Mexico and Caribbean Oil Spill in Coastal Ecosystems: Assessing effects, natural recovery, and progress in remediation research* (pp. 55–61). New Orleans, LA: US Department of the Interior, Minerals Management Service (OCS Study/MMS 95-0063).
- Wettle, M., Daniel, P.J., Logan, G.A., & Thankappan, M. (2009). Assessing the effect of hydrocarbon oil type and thickness on a remote sensing signal: A sensitivity study based on the optical properties of two different oil types and the Hymap and Quickbird sensors. *Remote Sensing of Environment*, 113, 2000–2010.